J Supercond Nov Magn (2016) 29:2395–2400
DOI 10.1007/s10948-016-3533-z

ORIGINAL PAPER

The Effect of Cr^{3+} Substitution on Magnetic Properties of $CoFe_2O_4$ Nanoparticles Synthesized by Microwave Combustion Route

A. Baykal[1] · Ş. Eryiğit[1] · M. Sertkol[2] · S. Ünlü[1] · A. Yıldız[3] · Sagar E. Shirsath[4]

Received: 24 February 2016 / Accepted: 27 April 2016 / Published online: 27 May 2016

Abstract $CoCr_xFe_{2-x}O_4$ ($0.0 \leq x \leq 1.0$) nanoparticles were synthesized by a microwave combustion method and the effect of Cr^{3+} substitution on structural, morphological, and magnetic properties of $CoFe_2O_4$ was studied. The structural, morphological, and magnetic properties of the products were determined and characterized in detail by X-ray diffraction (XRD), high-resolution scanning electron microscopy (HR-SEM), energy-dispersive X-ray spectroscopy (EDX), Fourier transform infrared spectroscopy (FT-IR), and vibrating sample magnetometer (VSM). Cation distribution of calculations confirmed the B site (octahedral site) preference of substituted Cr^{3+} ions. X-ray analysis showed that all compositions crystallize with a cubic spinel-type structure. The lattice parameter decreased from 8.384 to 8.362 Å with increasing Cr content. The average crystallite size was found in the range of 30.6–45.4 nm. Magnetization measurements showed that saturation magnetization of products decreases with the increase of the Cr substitution (x).

Keywords $CoFe_2O_4$ · Cation distribution · Magnetic properties · Cr substitution

✉ A. Baykal
hbaykal@fatih.edu.tr

[1] Department of Chemistry, Fatih University, 34500 Büyükçekmece/İstanbul, Turkey

[2] Department of Physics Engineering, Istanbul Technical University, 34469, Maslak, İstanbul, Turkey

[3] Department of Textile Engineering, Namık Kemal University, 59860 Çorlu-Tekirdağ, Turkey

[4] Spin Device Technology Center, Faculty of Engineering, Shinshu University, 380-8553 Nagano, Japan

1 Introduction

Cobalt ferrite is an important compound due to its strong magnetic anisotropy [1], high coercivity at room temperature [2], moderate saturation magnetization [3], magnetostriction [4], and good mechanical and chemical stability [5, 6]. $CoFe_2O_4$ is a promising material for high-density recording of its excellent electrical and magnetic properties.

The addition of a small amount of impurity (metal ions with different valence states) leads to effective modification in the electrical and magnetic properties of spinel ferrites [7] because these types of additions lead to various tetrahedral (A) and octahedral (B) site distributions [8, 9]. Hence, the change in cation distribution affects the physical properties of spinel ferrites.

Up to now, various methods have been used for the synthesis of Cr^{3+}-substituted cobalt ferrite nanoparticles. Iqbal and Siddiquah [10] used a micro-emulsion method using polyethylene glycol (PEG) as a surfactant at pH 9.50. Hankarea et al. [11] synthesized the spinel-phase nanocrystalline $CoCr_xFe_{2-x}O_4$ powders ($0.0 \leq x \leq 2.0$) by a citrate-gel precursor method. Singhal et al. [7] and Toksha et al. [12] synthesized the $CoCr_xFe_{2-x}O_4$ powders ($0.0 \leq x \leq 2.0$) by a sol-gel auto-combustion method. Vadivel et al. [9] and Kumari et al. [13] produced the Cr-substituted $CoFe_2O_4$ nanoparticles (NPs) by a coprecipitation method. Lastly, Panda et al. [14] investigated the effect of incorporation of Cr^{3+} into $CoFe_2O_4$ NPs on its magnetic and electric properties, prepared by a auto-combustion method.

Literature survey reveals that no systematic studies are available on the synthesis of Cr-substituted $CoFe_2O_4$ NPs by a microwave combustion method. Therefore, in the present investigation, pure and Cr-substituted $CoFe_2O_4$ NPs were prepared by the combustion method for various

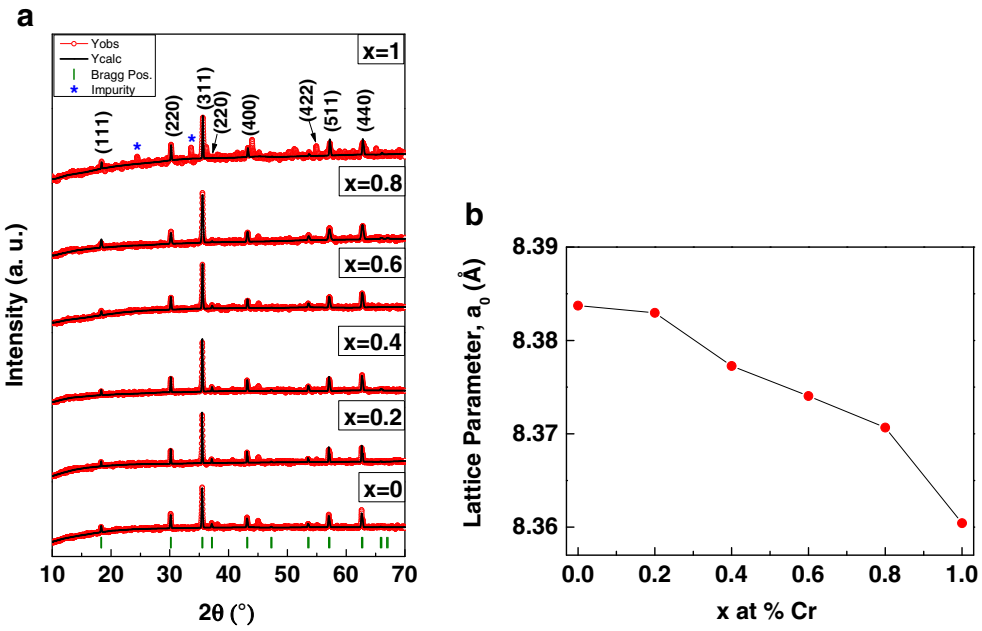

Fig. 1 **a** XRD spectra with Rietveld analysis patterns. **b** Lattice constant a_o (Å) with Cr concentration varying with x for $CoCr_xFe_{2-x}O_4$ ($0.0 \leq x \leq 1.0$) NPs

concentrations of Cr. The effect of Cr concentration on structural, spectral, morphological, and magnetic properties is reported in the present work.

2 Experimental

2.1 Chemicals and Instrumentation

Analytical grade chemical reagents $Co(NO_3)_2{\cdot}6H_2O$, $Cr(NO_3){\cdot}9H_2O$, and $Fe(NO_3)_3{\cdot}9H_2O$, and citric acid monohydrate, $C_6H_8O_7{\cdot}H_2O$ (as fuel), were obtained from Merck and used without further purification process.

The crystalline structure of resultant nanoparticles was determined with X-ray diffraction (XRD) measurements using Rigaku D/Max-IIIC with Cu-Kα radiation in the 2θ range of 20°–70°.

Fourier transform infrared spectroscopy (FT-IR) spectra were recorded in transmission mode with a PerkinElmer BX FT-IR infrared spectrometer. FT-IR spectra in the range of 4000–400 cm^{-1} were recorded in order to investigate the nature of the chemical bonds formed.

The surface morphology of the composites was analyzed with JEOL JSM-7001F scanning electron microscopy (SEM).

Magnetic measurements were performed by using a Quantum Design vibrating sample magnetometer (QD-VSM). The sample was measured at ±10 kOe at room temperature (25 °C).

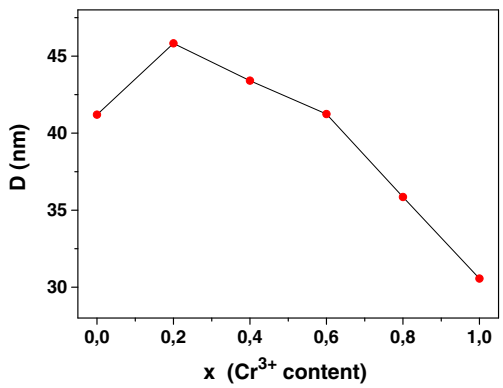

Fig. 2 Particle size analysis for $CoCr_xFe_{2-x}O_4$ ($0.0 \leq x \leq 1.0$) NPs estimated by the Scherrer method from (311) peak

2.2 Procedure

Nanocrystalline powders of $CoCr_xFe_{2-x}O_4$ ($0.0 \leq x \leq 1.0$) were synthesized by a microwave method. For each experiment, a stoichiometric amount of metal salts and 1 g citric acid were taken and ground in an agate mortar

Table 1 Cation distribution of $CoCr_xFe_{2-x}O_4$ ($0.0 \leq x \leq 1.0$) NPs

x	Tetrahedral A site	Octahedral B site
0.0	$Co_{0.2}Fe_{0.8}$	$Co_{0.8}Fe_{1.2}$
0.2	$Co_{0.2}Fe_{0.8}$	$Co_{0.8}Cr_{0.2}Fe_{1.0}$
0.4	$Co_{0.25}Fe_{0.75}$	$Co_{0.75}Cr_{0.4}Fe_{0.85}$
0.6	$Co_{0.25}Fe_{0.75}$	$Co_{0.75}Cr_{0.6}Fe_{0.65}$
0.8	$Co_{0.3}Fe_{0.7}$	$Co_{0.7}Cr_{0.8}Fe_{0.5}$
1.0	$Co_{0.3}Fe_{0.7}$	$Co_{0.7}Cr_{1.0}Fe_{0.3}$

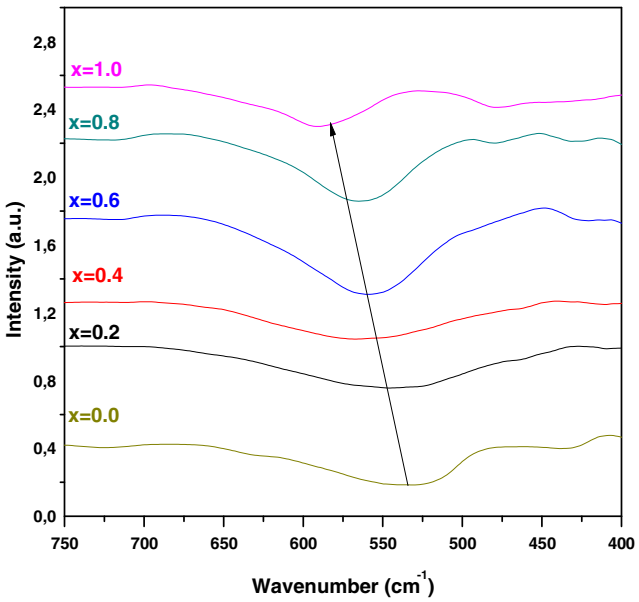

Fig. 3 FT-IR spectra of $CoCr_xFe_{2-x}O_4$ ($0.0 \leq x \leq 1.0$) NPs

for 10 min and then they were placed into a commercial microwave oven. At the beginning of the reaction, there was gas evolution from the crucible and then the color of the reactant mixture turned into red color due to the high temperature inside the oven. Unfortunately, it was possible to measure the temperature inside the oven during the chemical reaction which was completed in 5 min. Then, the solid product was washed with distilled water-ethanol and dried at 150 °C to remove remaining water contents.

3 Results and Discussion

3.1 XRD Analysis

The XRD powder patterns and variation of lattice constants with Cr concentration (x) of $CoCr_xFe_{2-x}O_4$ ($0.0 \leq x \leq 1.0$) NPs are presented in Fig. 1a, b, respectively. The XRD powder patterns indicate that all products contain single-phase spinel cubic structure (Fig. 1a) (except for $x = 1.0$ which contains a small amount of impurity). The XRD peaks of all products can be indexed to the spinel cubic structure of $CoFe_2O_4$ (ICDD card no: 03-0864) [15]. It is observed that lattice parameter goes on decreasing from 8.384 Å ($x = 0.0$, $CoFe_2O_4$) to 8.362 Å ($x = 1.0$, $CoCrFeO_4$) with increasing Cr content (x). The decrease of a_o with an increase in x is due to the fact that the larger ionic radii of Fe^{3+} (0.67 Å) are replaced by smaller ionic radii of Cr^{3+} (0.63 Å) (Fig. 1b). Therefore, the lattice parameter decreases because of shrinkage of unit cell dimension. This indicates a difference of Fe^{3+} and Cr^{3+} in an oxide solid solution with a spinel-type structure [9, 12]. The variation of lattice parameters with x for all products obeys Vegard's law [16]. This observation is in good agreement with the reports given in the literature [9, 12, 17, 18]. The variation of crystallite sizes with x is presented in Fig. 2.

3.2 Cation Distribution

Site occupancy of all constituent ions in $CoCr_xFe_{2-x}O_4$ ($0.0 \leq x \leq 1.0$) NPs is presented in Table 1. It is observed that $CoFe_2O_4$ ($x = 0.0$) shows an inverse spinel structure where most of the divalent Co ions occupy octahedral B site

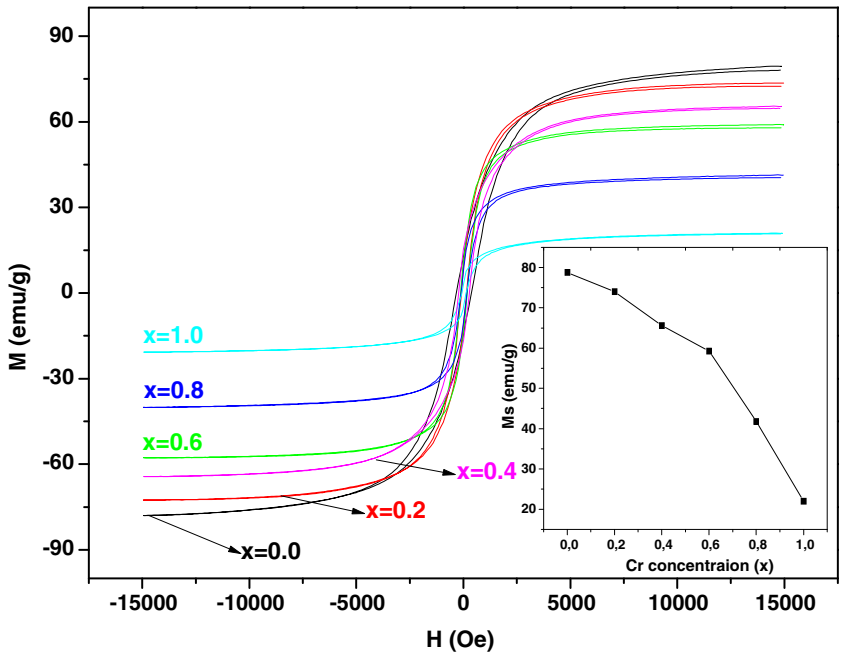

Fig. 4 Magnetic hysteresis loops of $CoCr_xFe_{2-x}O_4$ ($0.0 \leq x \leq 1.0$) NPs at RT (the *inset* shows the variation of M_s with Cr substitution (x))

and Fe ions are randomly distributed over both the sites. As the Cr^{3+} substitution in $CoFe_2O_4$ increased, it prefers to occupy the octahedral B site only. As the substitution level of Cr^{3+} ion increased, it pushes some of the Co ions to the tetrahedral A site. However, throughout the substitution level, Co ions show preference toward the octahedral B site along with Cr^{3+} ions.

3.3 FT-IR Analysis

The FT-IR spectra of $CoCr_xFe_{2-x}O_4$ ($0.0 \leq x \leq 1.0$) NPs are presented in Fig. 3 which showed that all products have two prominent absorption bands, ν_1 (due to the stretching of tetrahedral metal ion and oxygen bonding) and ν_2 (vibrations of oxygen in the direction perpendicular to the axis joining the tetrahedral ion and oxygen), in the range of 600–500 and 430–385 cm^{-1}, respectively [9, 12, 19]. As it can be seen from Fig. 3, the Fe–O bands towards higher frequency with an increase in concentration of Cr^{3+} ions [9, 11, 20].

3.4 VSM Analysis

The room-temperature M–H graphs of $CoCr_xFe_{2-x}O_4$ ($0.0 \leq x \leq 1.0$) NPs are presented in Fig. 4. The substitution of some trivalent nonmagnetic ions for Fe^{3+} in spinel ferrites is made for special magnetic and electrical function. From Fig. 4, it can be noticed that the saturation magnetization (~79 emu/g which is in good agreement with the reported values [20]) is high for $CoFe_2O_4$ ($x = 0.0$) NPs and it decreases gradually with increasing Cr concentration (x) (the saturation magnetization, M_s, decreases from

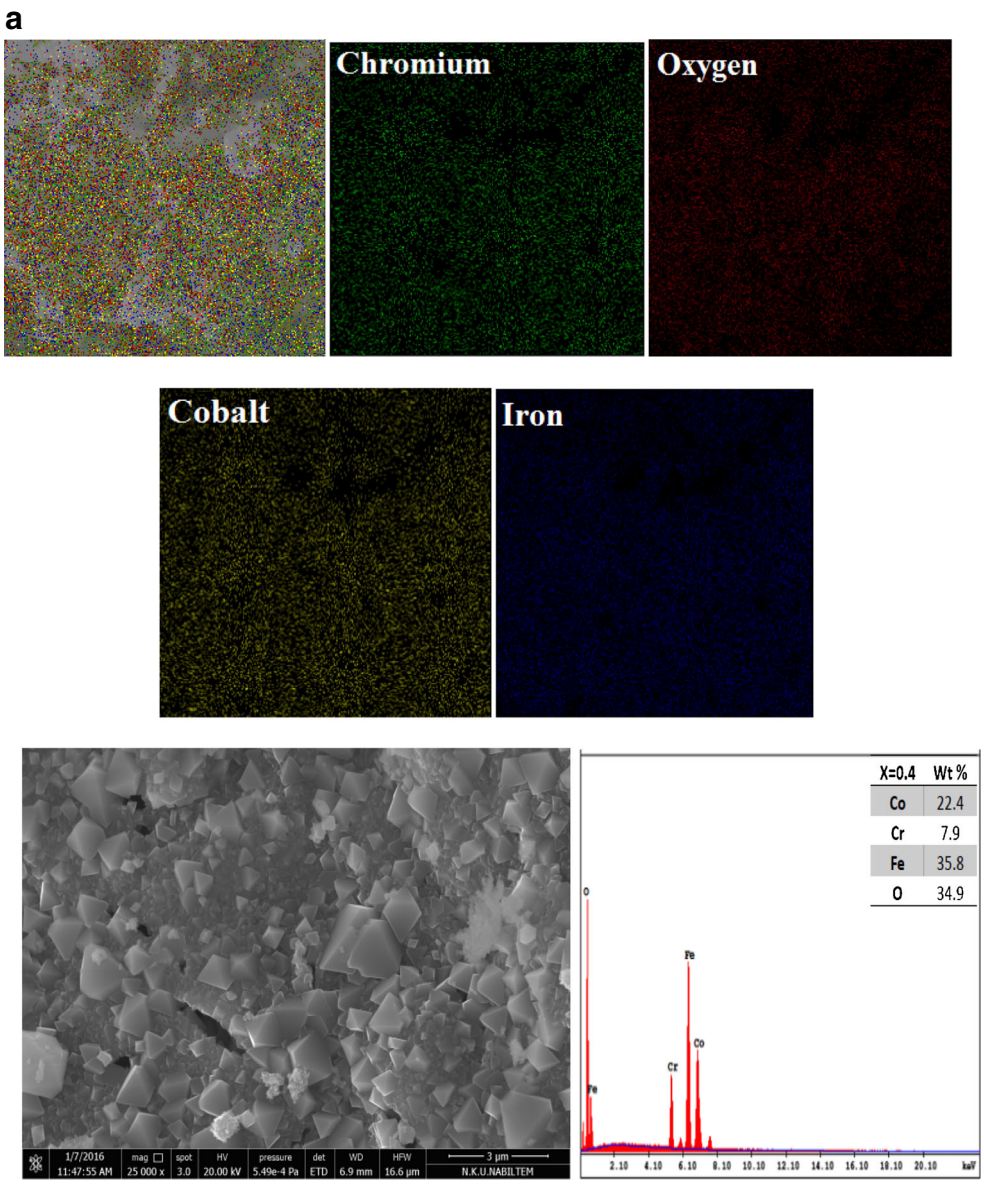

Fig. 5 SEM image, EDX spectrum, and elemental map of **a** $CoCr_{0.4}Fe_{1.6}O_4$ and **b** $CoCr_{0.8}Fe_{1.2}O_4$ NPs

Fig. 5 (continued)

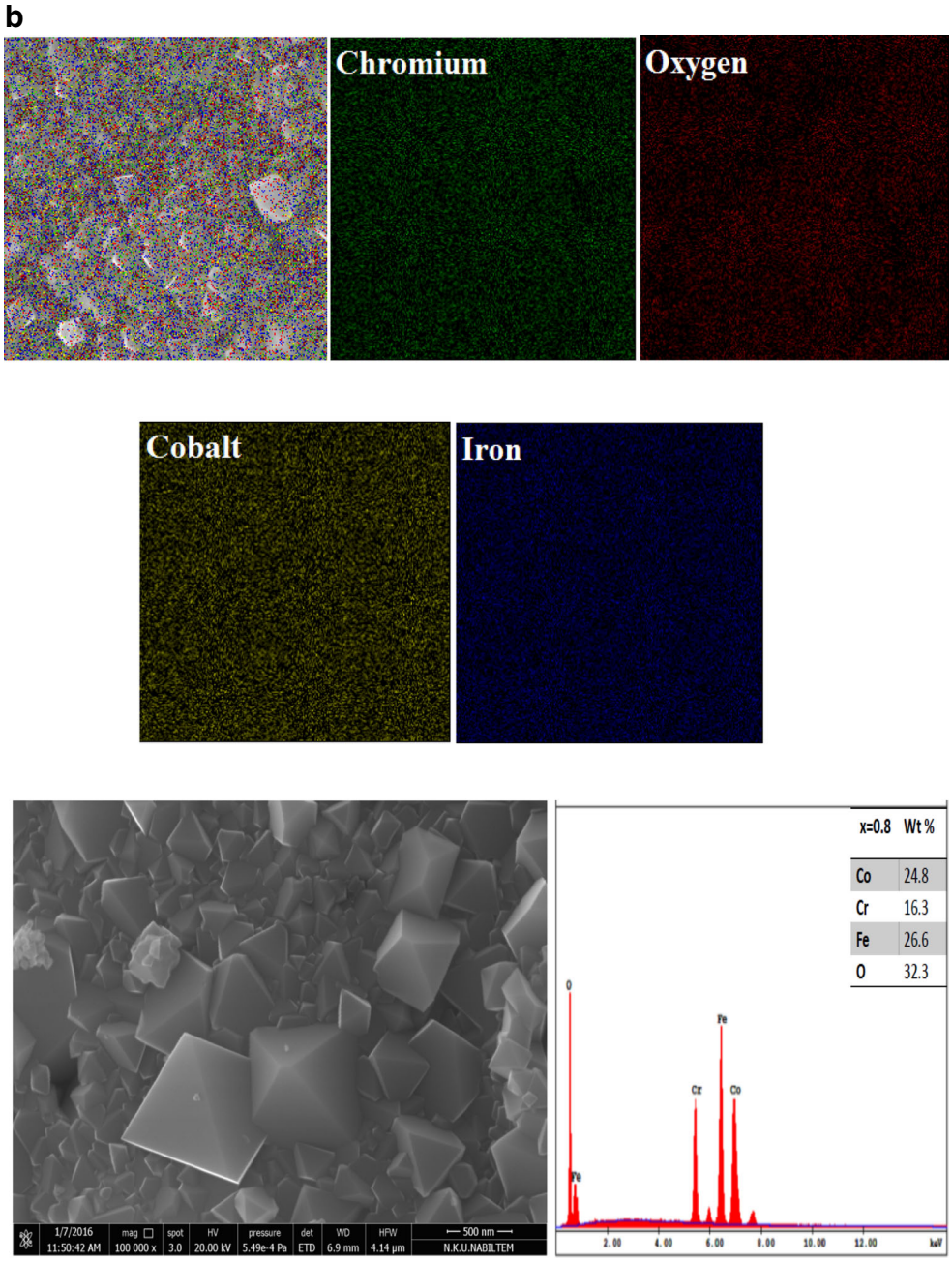

79 to 21.4 emu/g with the increase in Cr^{3+} concentration) (Fig. 4, inset). This observation can be explained as follows: The introduction of nonmagnetic ions on octahedral B sites in the inverse spinel cobalt ferrite will reduce the saturation magnetization since it has a net uncompensated moment and alters their magnetic and electric properties [18]. As it was stated in various reports [11, 14], there is replacement of Fe^{3+} ions ($3d^5$, magnetic moment 5 μ_B) by lesser magnetic Cr^{3+} ions ($3d^8$, magnetic moment 3 μ_B) in the octahedral sites [9]. The substitution of Cr^{3+} into B site (octahedral site) was also confirmed by the cation distribution calculations above.

3.5 SEM and Energy-Dispersive X-ray Spectroscopy Analysis

The SEM micrographs, the energy-dispersive X-ray spectroscopy (EDX) spectra (along with elemental percentage of each element, O, Co, Cr, and Fe), and the elemental maps (including the mapping of the cation distributions) of $CoCr_{0.4}Fe_{1.6}O_4$ and $CoCr_{0.8}Fe_{1.2}O_4$ NPs are presented in Fig. 5a, b, respectively. The cubic morphology can be clearly seen for both products. It also shows the presence of a large agglomeration phenomenon in the grains, which might be caused by the high temperature during

the microwave irradiation for both products. The average particle size of both products is in the range of 100–200 nm. Values of the particle sizes differ significantly from those determined from XRD powder patterns due to the agglomeration. The SEM-EDX results confirmed the formation of exact composition of spinel-type chromium-substituted cobalt ferrite spinel compounds (for all products) with O, Co, Cr, and Fe elements, and no impurity is present in the products [21–24]. Figure 5 shows the representative X-ray elemental maps of all elements detected in EDX, that is, oxygen, chromium, cobalt, and iron, in $CoCr_{0.4}Fe_{1.6}O_4$ and $CoCr_{0.8}Fe_{1.2}O_4$ NPs. Both maps indicate fairly homogeneous elemental distributions in both products.

4 Conclusion

Pure and Cr-doped cobalt ferrite nanoparticles were successfully prepared by the microwave combustion method from nitrate salts of Co, Cr, and Fe using citric as fuel. The crystallite size was found to vary slightly from 30.6 to 45.8 nm. The formation of single and pure spinel phase was confirmed by the Rietveld analysis. The lattice parameter is reduced from 8.384 to 8.362 Å by Cr^{3+} substitution, leading to the contraction of the unit cell volume. The decrease in lattice constant is due to the smaller ionic radii of the doped cation Cr^{3+} (0.63 Å) compared to that of Fe^{3+} (0.67 Å). Fe^{3+} was replaced at B site (octahedral) by Cr^{3+} that weakened the magnetic interaction among cations and which caused a decrease in saturation magnetization. Spinel ferrites are widely used in microwave devices due to their high resistivity, and the substitution of Cr^{3+} increases the resistivity due to the octahedral B site preference of Cr^{3+}. Hence, these materials can be used in microwave devices also. Hence, as a further study, the resistivity studies related to these products are still going on.

Acknowledgments This study is supported by the Fatih University under BAP grant no. P50031504_B.

References

1. Ortega, A.L., Lottini, E., Fernandez, C.J., Sangregorio, C.: Chem. Mater. **27**, 4048–4056 (2015)
2. Chinnasamy, C.N., Jeyadevan, B., Shinoda, K., Tohji, K., Djayaprawira, D.J., Takahashi, M., Joseyphus, R.J., Narayanasamy, A.: Appl. Phys. Lett. **83**, 2862–2864 (2003)
3. Wang, Y.C., Ding, J., Yin, J.H., Liu, B.H., Yi, J.B., Yu, S.: J. Appl. Phys. **98**, 124306 (2005)
4. Wang, J., Gao, X., Yuan, C., Li, J., Bao, X.: J. Magn. Magn. Mater. **401**, 662–666 (2016)
5. Qu, Y., Yang, H., Yang, N., Fan, Y., Zhu, H., Zou, G.: Mater. Lett. **60**, 3548 (2006)
6. Kasapoğlu, N., Baykal, A., Köseoğlu, Y., Toprak, M.S.: Scr. Mater. **57**, 441–444 (2007)
7. Singhal, S., Jauhar, S., Singh, J., Chandra, K., Bansal, S.: J. Mol. Struct. **1012**, 182 (2012)
8. Gul, I.H., Maqsood, A.: J. Alloys Compd. **465**, 227 (2008)
9. Vadivel, M., Ramesh Babu, R., Sethuraman, K., Ramamurthi, K., Arivanandhan, M.: J. Magn. Magn. Mater. **362**, 122–129 (2014)
10. Iqbal, M.J., Siddiquah, M.R.: J. Alloy Compd. **453**, 513–518 (2008)
11. Hankarea, P.P., Sankpal, U.B., Patil, R.P., Mulla, I.S., Lokhandec, P.D., Gajbhiye, N.S.: J. Alloy Compd. **485**, 798–801 (2009)
12. Toksha, B.G., Shirsath, S.E., Mane, M.L., Patange, S.S., Jadhav, S.S., Jadhav, K.M.: J. Phys. Chem. C **115**, 20905–20912 (2011)
13. Kumari, N., Kumar, V., Singh, S.K.: Cer. Int. **40**, 12199–12205 (2014)
14. Panda, R.K., Muduli, R., Jayarao, G., Sanyal, D., Behera, D.: J. Alloy Compd. **669**, 19–28 (2016)
15. Manikandan, A., Sridhar, R., Antony, S.A., Ramakrishna, S.: J. Mol. Struct. **1076**, 188–200 (2014)
16. Vegard, L.: Z. Phys. **15**, 17–26 (1921)
17. Mane, D.R., Patil, S., Birajdar, D.D., Kadam, A.B., Shirsath, S.E., Kadam, R.H.: Mater. Chem. Phys. **126**, 755–760 (2011)
18. Chae, K.P., Lee, Y.B., Lee, J.G., Lee, S.H.: J. Magn. Magn. Mater. **220**, 59–64 (2000)
19. Waldron, R.D.: Phys. Rev. **99**, 1727–1735 (1955)
20. Singhal, S., Barthwal, S.K., Chandra, K.: J. Magn. Magn. Mater. **306**, 233–240 (2006)
21. Khalaf, K.A.M., Al-Rawas, A.D., Widatallah, H.M., Al-Rashdi, K.S., Sellai, A., Gismelseed, A.M., Hashim, M., Jameel, S.K., Al-Ruqeishi, M.S., Al-Riyami, K.O., Shongwe, M., Al-Rajhi, A.H.: J. Alloy Compd. **657**, 733–747 (2016)
22. Padmaraj, O., Venkateswarlu, M., Satyanarayana, N.: Ceram. Int. **41**, 3178–3185 (2015)
23. Wu, K., Hu, G., Du, K., Peng, Z., Cao, Y.: Synthesis and electrochemical characterization of $LiCo_{1/3}Fe_{2/3}PO_{4/C}$ composite using nano $CoFe_2O_4$ as precursor. J. Alloy Compd. **650**, 718–723 (2015)
24. Baykal, A., Elmal, A.Z., Sertkol, M., Sözeri, H.: J. Supercond. Nov. Magn. **28**, 3405–3410 (2015)